Exploring Electonic Structure and Spectral Properties of Nitrogen-Doped Boron Clusters B_nN with $n = 10 - 20$

Cheng-Hong Deng[*], Zheng-Wen Long[†], Yue-Ju Yang[‡], Shi-Xiong Li[§]

June 14, 2022

Abstract

For a better understanding the effects of nitrogen atom doping on boron clusters, we investigated adopting the ABCluster global search technique and CALYPSO approach combined with density functional theory the lowest energy structures, bonding, electrons delocalization and spectral properties of neutral nitrogen-doped boron clusters, the size of which varies from 10 to 20. The results of its calculations are displayed the global minimum of these clusters are plane or quasi plane structures at $n = 11, 13, 15-20$, the bowl-like structures at $n = 10, 12$ and the boat-shaped structure at $n = 14$. It is found that $B_{20}N$ is most stable of all structures. Natural population analysis (NPA) indicates that boron atoms sectional electrons transfer to doped nitrogen atoms. Electron localization Orbital Function (LOL) and Electron Localization Function (ELF) analysis indicate that there are strong covalent bonds between doped N atons and B atoms for clusters $B_nN(n = 10 - 20)$. In addition, under the same isosurface, the isosurface of $B_{10}N$ is the thickest, indicating that it has the most electrons and the strongest delocalization. Infrared and Raman spectra show that clusters $B_nN(n = 10-20)$ have a great deal of characteristic peaks, and the strongest IR peaks and Raman peaks are situated at different positions, which can be used to identify the clusters structures and make comparative analysis with future experiments. Electronic absorption spectrum analysis shows that the first absorption peak of these clusters is located in the visible band. The study provides theoretical guidance and basis for the development of novel boron-based nanomaterials.

[*]Department of physics, Guizhou University, Guiyang
[†]Department of physics, Guizhou University, Guiyang (Corresponding author)
[‡]School of Physics and Electronic Science, Guizhou Education University, Guiyang
[§]School of Physics and Electronic Science, Guizhou Education University, Guiyang

1. INTRODUCTION

Clusters are relatively stable microscopic or submicroco aggregates composed of a certain number of atoms, molecules, or ions in a certain bonding manner [1, 2]. it is an important bridge connecting microscopic atoms and macroscopic materials, and its geometric structure, electronic properties and novel physicochemical properties have opened up a new direction for the production of special performance materials, as a result, it has received widespread attention.

As the first light element with a 2p electron in the periodic table, the boron atom can form multicenter chemical bonds due to its electron-deficient characteristics, thus exhibiting extraordinary properties [3–5]. In recent decades, a great deal of researches have been conducted around pure boron clusters and their doped boron clusters [5, 34]. Theoretical and experimental results show clusters B_n^- with atomic number 38 or less possess planar or quasi-planar structures of central pentagonal, hexagonal and heptagonal pores [3, 6], of which the discovery of quasi-planar structure B_{36}^- [37] provides feasibility for the experimental synthesis of borospherene [7–9, 32] and these polygonal pores play a crucial role in the stability of two-dimensional boron clusters [15].

In 2014, firstly determined the first caged full boron cluster $B_{40}^{-/0}$ with high stability by using photoelectron spectroscopy experiment combined with quantum chemistry theory, named "borospherene" [10–12, 31]. It is found that there are energy competition between the two-dimensional (2D) and three-dimensional (3D) structures of borospherene $B_{40}^{-/0}$, and smaller anionic boron clusters are preferring two-dimensional structures [13]. For neutral pure boron clusters, the small boron clusters B_n ($n = 2 - 19$) are two-dimensional (2D) structures formed on the basis of B_3 units, in addition to the boron cluster B_{14} of the cage structure [35]. Among them, the boron-based nanosystem with low dimension can be regard as composed of B_3 triangular structural units and boron double-chains [46]. The presence of the B_3 ring coincides with the electron-deficient property of the boron atom itself, which is easy to form delocalization bond and is generally considered aromatic [46, 59]. For boron clusters of certain sizes, tubular structures are more advantageous, such as B_{40} of the fullerene cage structure having the lowest energy structure, can be seen as a boron analogue of C_{60}

[14, 15, 42]. Cage-like B_{80} and all-boron nanosheets are the most promising materials for capturing and storing industrial gases [25, 58], such as hydrogen and carbon dioxide. Therefore, systematically investigate of the geometry, stability and bonding of boron clusters for a certain size, as well as their evolution with size, is a necessary basis for the discovery of novel nanomaterials.

In the last dozen years, researchers have been carried out many studies on boron clusters doped by transition metals or main group elements, the results show that the drum-like CoB_{16}^{-} cluster with central Co aton is connected by two B_8 rings, and it has high symmetry, is the highest coordination number known to in chemistry, so far [16–18]. It is exciting that the structure of pure boron cluster B_{24} is generally quasi planar structure and irregular polyhedral structure, while the doping Mo or W elements in boron cluster B_{24} form that endohedral structure with high symmetry of D_{3h}, and has strong thermodynamic, dynamics and chemical stability [19, 20, 33, 40]. Chemical bonding analysis revealed that the transition metal-doped nine-membered boron rings M©B_9 and M©B_9^{-}(M=Rh, Ir) are diaromatic, with each of these compounds having six delocalized π electrons and α electrons which describe the bonding mode between central metal atoms and boron rings [21, 22, 36, 41]. In theory, chemical bonding and aromatic properties of several mixed clusters of B_nM (M=Be, Na, Li) have been systematically studied [23, 24]. Similar theoretical studies have been made about the aluminum-doped boron cluster AlB_n [25]. First-principles studies have found that there is a strong covalent and molecular properties between molecules of mixed clusters $(AsB)_n (n = 1 - 14)$ [26]. Studies on the activities of endogram and exosome M&B_{40}(M=Be, Mg) and M@B_{40} (M=Ca, Sr) have also been reported [48, 49]. The effects of doping of the main groups S, P and C on the structures, bonding properties and thermodynamic stability of small boron clusters have been extensively studied [27, 28]. As can be seen from the above, the effects of doping of metallic elements, transition metal elements and some non-metallic elements on boron clusters have been comprehensive reported [29].

However, the nitrogen as a nonmetallic element whose valence electron configuration is $2s^2\ 2p^3$, its compounds have important applications in all aspects of life. For example, it can be used to make nitric acid and nitrogen fertilizers, which are widely used in agriculture. A boron atom and a nitrogen atom are combined to form boron nitride, which is high stability,

heat resistance and corrosion resistance, can be used to make high-temperature insulation materials, is widely used in the aerospace industry. Based on the unique physical and chemical properties of boron-containing compounds, it is of great significance to study nitrogen boron compounds of a certain size.

And, so far, there is no literature reporting on the effects of doping boron clusters of nitrogen, and this paper uses density functional theory to theoretically discuss the structures, bonding and spectral characteristics of B_nN ($n = 10 - 20$) clusters, hoping to provide theoretical guidance and basis for the development of novel boron based nanomaterials.

2. COMPUTATIONAL METHOD

The initial geometric structures of neutral B_nN clusters ($n = 10 - 20$) are obtained by using the ABCluster global search method [50–52] and particle swarm optimization (CALYPSO) software [53] combining with the Gaussian 09 program [54]. The first step is achieved preliminary structural search at PBE0 [39] level with 6-31G basis set. More than 2000 initial structures are obtained for each cluster size. The theoretical method selected is derived from previous studies on silicon-boron clusters [55, 56]. After the geometry optimizations, frequency analyses, electronic structures and spectroscopic properties are studied at PBE0 level with 6-311G(D) basis set.

Harmonic frequency analyses for B_nN clusters ($n = 10 - 20$) are performed at PBE0 method with 6-311G(D) to guarantee that the optimized structures are local minima. Localized orbital function (LOL) [45] and Electron localization function (ELF) [47, 48] are used to analyze chemical bonds, all kinds of isosurface maps are drawn by Multiwfn3.8 [44] and VMD [46] software. All results are calculated in Gaussian 09 software.

3. RESULTS AND DISCUSSION

3.1 Geometrial Structures

The initial structures of the nitrogen-doped boron clusters B_nN ($n = 10 - 20$) are obtained by using ABCluster and CALYPSO software to search for the global minimum value of the potential energy surface. The initial structures are optimized step by step under the density functional method PBE0 with 6-311G(D) basis set to determine the structures with the lowest energy, Figure 1 shows its lowest energy structure and its corresponding electronic states and symmetries.

Table 1: The symmetries, state, structures of $B_nN(n = 10 - 20)$

clusters	symmetry	state	structure
$B_{10}N$	C_1	^2A	bowl-shaped structure
$B_{11}N$	C_1	^1A	plane structure
$B_{12}N$	C_1	^2A	bowl-shaped structure
$B_{13}N$	C_{2v}	$^1A_1$	plane structure
$B_{14}N$	C_1	^2A	boat-shaped structure
$B_{15}N$	C_s	$^1A'$	plane structure
$B_{16}N$	C_s	$^2A'$	plane structure
$B_{17}N$	C_1	^1A	plane structure
$B_{18}N$	C_s	^2A	plane structure
$B_{19}N$	C_s	^2A	plane structure
$B_{18}N$	C_s	^2A	plane structure
$B_{19}N$	C_s	^1A	plane structure
$B_{20}N$	C_s	$^2A''$	plane structure

The symmetries and electronic states information of the most relevant metastable structures have exhibited in Figure S1 (Support Information). For metastable structures, it can be seen from these clusters that $B_nN(n = 10, 11, 13 - 17, 20)$ are plane structres, $B_{12}N$ is a

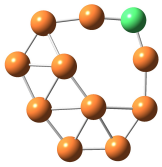

$B_{10}N$

$C_1\ ^2A$

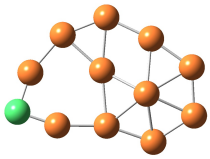

$B_{11}N$

$C_1\ ^1A$

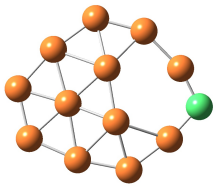

$B_{12}N$

$C_1\ ^2A$

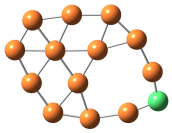

$B_{13}N$

$C_{2v}\ ^1A_1$

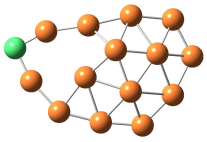

$B_{14}N$

$C_1\ ^2A$

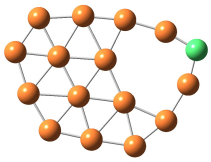

$B_{15}N$

$C_s\ ^1A'$

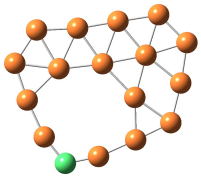

$B_{16}N$

$C_s\ ^2A'$

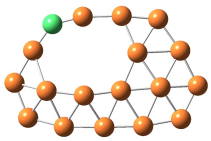

$B_{17}N$

$C_1\ ^1A$

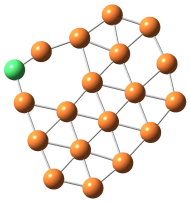

$B_{18}N$

$C_s\ ^2A$

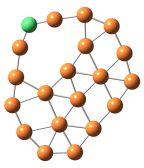

$B_{19}N$

$C_s\ ^1A$

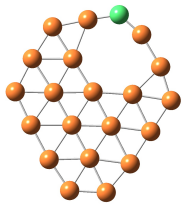

$B_{20}N$

$C_s\ ^2A''$

Figure 1: The lowest energy geometries of clusters $B_nN(n = 10 - 20)$.

boat-shapes structre, $B_{18}N$ and $B_{19}N$ are three dimensional structures. Compared with the lowest energy structures, there are different, but they are still mainly plane structures.

From Figure 1 and Table 1 know that B_nN clusters ($n = 10, 12, 14$) no longer have a planar or quasi planar structures with N atoms doping, while presenting three-dimensional structures. The $B_{10}N$ and $B_{12}N$ clusters are bowl-like structures formed by replacing a boron atom with a nitrogen atom in the B_{11} and B_{13} clusters of planar structures, respectively. While $B_{14}N$ is a boat-shaped structure with a nitrogen atom located at the bow, similar to what has been reported for MgB_{10} cluster [57]. Their lowest energy structures are dominated by the lowest spin (single or doubet).

The results show that the addition of a nitrogen atom has a great influence on pure boron clusters. In order to further analyze the frequency and electronic structures of the nitrogen-doped boron clusters BnN ($n = 10 - 20$), the lowst harmonic frequencies are given in Table 2, which can be seen the lowest energy structures obtained are most stable, because their vibrations do not appear negative frequencies.

3.2 The HOMO-LUMO Gaps and Charge Transfer

To better understand some ground-state parameters of the nitrogen atom-doped boron clusters B_nN ($n = 10 - 20$), some useful information is given in Table 2, including symmetries, electron states, dipole moments, lowest resonance frequencies, and atomic charges on the nitrogen-doped atoms, as well as the energy gaps E_g (E_L-E_H) between the highest occupying orbital (HOMO) and the lowest empty orbital (LOMO).

Figure 2 only shows the orbital plot of the highest occupied orbit and the lowest empty orbit for the closed shell structures, the value of E_g reflects the ability of an electron to jump from a occupied orbit to an empty orbit. the smaller the E_g value, indicating that the weaker its transition ability, the more stable its structure. As can be seen from Table 2, the energy gap value of $B_{11}N$, $B_{13}N$, $B_{15}N$, $B_{17}N$ and $B_{19}N$ are 2.96, 2.71, 2.59, 2.57 and 2.39, respectively. The results show that the energy gap values of $B_{19}N$ cluster is minimum, indicating that its structure is the most stable for the closed shell structures. It can be seen that the energy gaps value of clusters $B_nN(n = 11, 13, 15, 17, 19)$ decreases with the increase

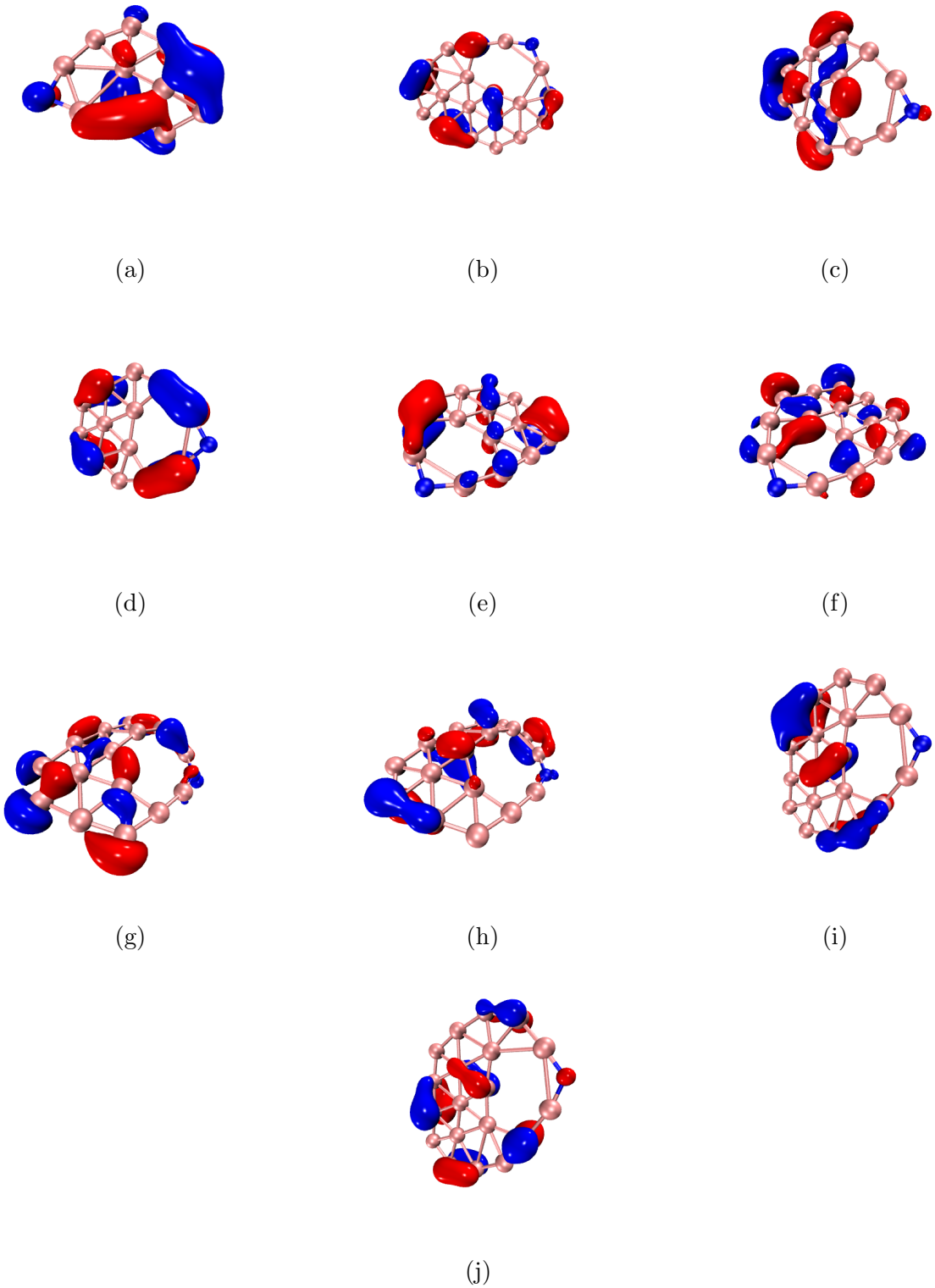

Figure 2: Molecular orbital graph. (a)HOMO $B_{11}N$; (b)LUMO $B_{11}N$; (c)HOMO $B_{13}N$; (d)LUMO $B_{13}N$; (e)HOMO $B_{15}N$; (f)LUMO $B_{15}N$; (g)HOMO $B_{17}N$; (h)LUMO $B_{17}N$; (i)HOMO $B_{19}N$; (j)LUMO $B_{19}N$.

Table 2: Dipole Moments(μ), Energy Gaps (E_g), Lowest Frequencies, and Charges on N Atoms of clusters $B_nN(n = 10 - 20)$.

cluster	μ/Debye	E_g /ev	lowst frequency (cm^{-1})	charges on N atoms
$B_{10}N$	1.78	2.30^{α} 3.60^{β}	161	-0.262
$B_{11}N$	0.95	2.96	177	-0.222
$B_{12}N$	1.21	3.10^{α} 2.09^{β}	122	-0.269
$B_{13}N$	2.24	2.71	100	-0.251
$B_{14}N$	2.32	2.76^{α} 2.61^{β}	93	-0.226
$B_{15}N$	1.70	2.59	83	-0.246
$B_{16}N$	1.70	2.27^{α} 2.14^{β}	26	-0.257
$B_{17}N$	2.14	2.57	87	-0.284
$B_{18}N$	2.16	2.36^{α} 2.33^{β}	101	-0.251
$B_{19}N$	2.02	2.39	72	-0.277
$B_{20}N$	0.69	2.18^{α} 2.11^{β}	83	-0.290

of boron atoms, indicating that their transition ability gradually decrease and stability of the clusters increase.

According to natural population analysis (NPA) of doped atoms showed that charges on the N atoms of these clusters were -0.262, -0.222, -0.269, -0.251, -0.226, -0.246, -0.257, -0.284, -0.251, -0.277, -0.290, respectively, showing negative charges. It means that some of the charges from each B atom are transferred to the N atoms.

3.3 The Chemical Bonding Analysis

Figure 3 and Figure S2 (Support Information) show to plot of clusters B_nN ($n = 10 - 20$) valence electron localization orbital function (LOL), the localization orbital function can better describe the electron delocalization characteristics, in the case of the same isosurface, the thicker the isosurface, indicating that electrons are more likely to delimit to other regions, the thinner the isosurface, indicating that electrons delocation are relatively difficult. As shown in Figure 3, at the isosurface value of 0.5, there is no blank space around the N atoms

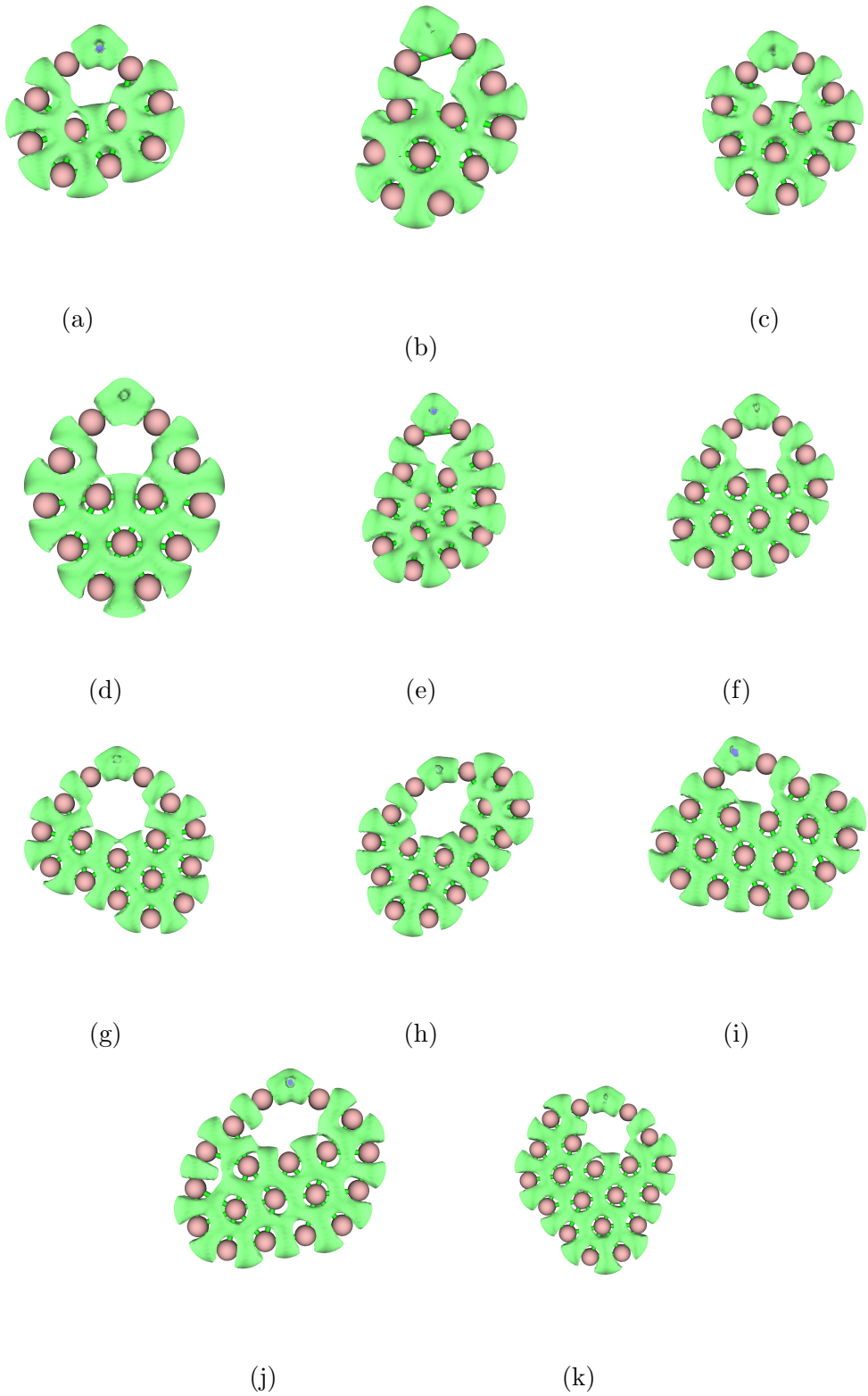

Figure 3: LOL with the isosurface of 0.5. (a)$B_{10}N$; (b)$B_{11}N$; (c)$B_{12}N$; (d)$B_{13}N$; (e)$B_{14}N$; (f)$B_{15}N$; (g)$B_{16}N$; (h)$B_{17}N$; (i)$B_{18}N$; (j)$B_{19}N$; (k)$B_{20}N$.

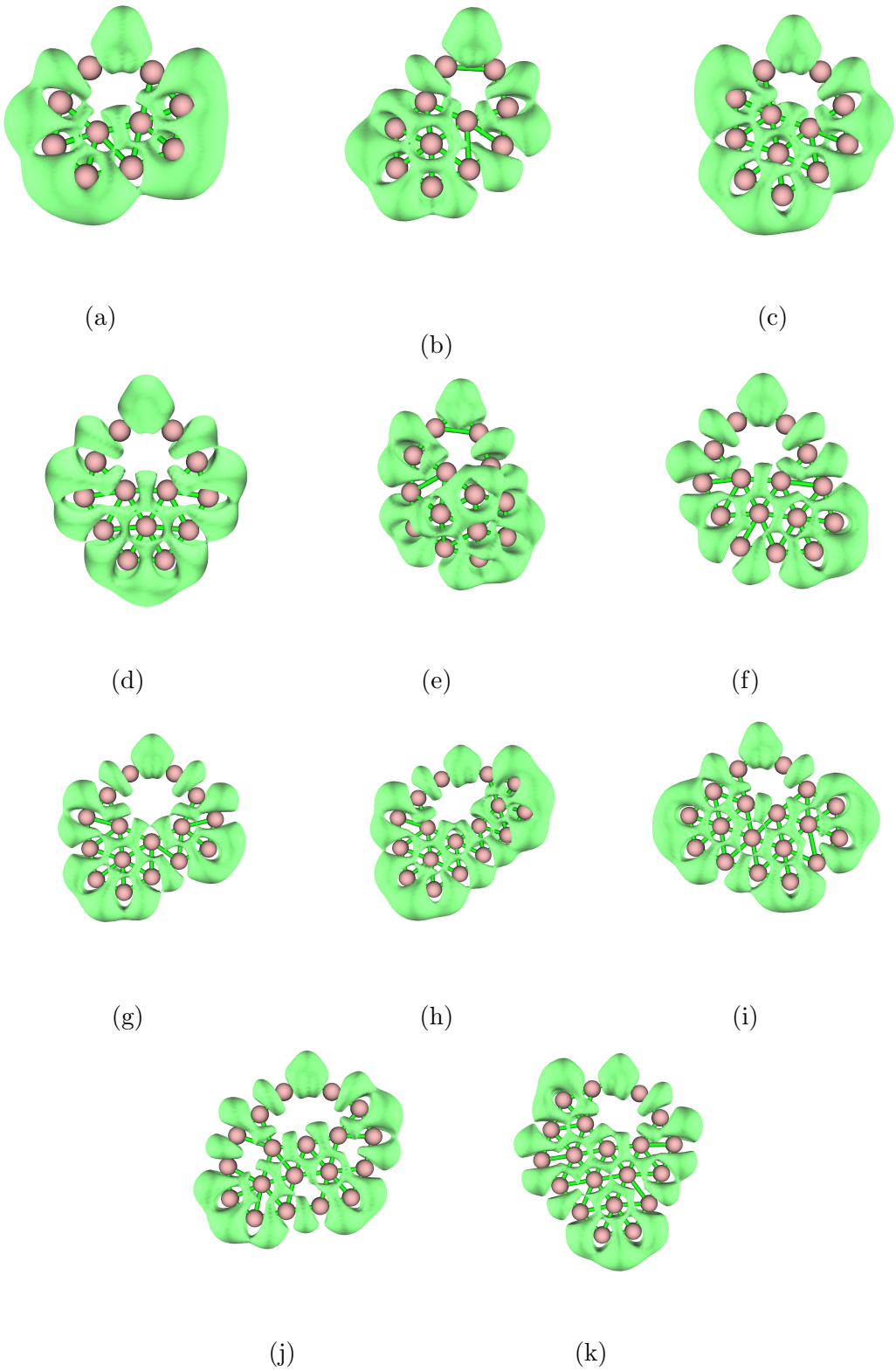

Figure 4: Electron localization function (ELF) with the isosurface of 0.7. (a)$B_{10}N$; (b)$B_{11}N$; (c)$B_{12}N$; (d)$B_{13}N$; (e)$B_{14}N$; (f)$B_{15}N$; (g)$B_{16}N$; (h)$B_{17}N$; (i)$B_{18}N$; (j)$B_{19}N$; (k)$B_{20}N$.

for B_nN ($n = 10-20$) clusters, indicating the formation of significant covalent bonds around the N and B atoms, and Figure S2 presents LOL plots with an isosurface of 0.6, at which point it can be seen that the isosurface of the clusters B_nN ($n = 10-20$) are broken at the N atoms, at this point, compared with the isosurface of 0.5, electron delocalization is stronger. As a result of the electron delocalization properties of these clusters, they are promised to become material primitives for molecular switches and molecular devices.

In order to further explore electronic localization and bonding properties of the clusters B_nN ($n = 10-20$), it is analyzed the electron localization function (ELF) of valence electrons, which is a measure of how well electrons are localized within different molecular regions. Figure 4 and Figure S3 (Support Information) show the electron density of under isosurface value at 0.7 and at 0.8, respectively. There is no a blank area near the N atoms, and there are forming strong covalent bonds between N atoms and B atoms, which showing no difference with the LOL discussion. Additionally, as the isosurface value increase, the characteristics of ELF and LOL become more and more similar. It can be seen from Figure 4 that the isosurface value is 0.7, the isosurface of $B_{10}N$ is the thickest, indicating that its electrons are easier to delocalize to other regions. Under the isosurface of 0.8, the isosurfaces are disconnected on the nitrogen atoms, indicating that electrons on the nitrogen atoms are reduced and the delocality is weakened. In the case of the same isosurfaces, the isosurface plot of the N atoms is thicker than the isosurface plot of the B atoms, showing that there are more electrons on N atoms and its electron density is greater.

3.4 Infrared and Ramam Spectral Properities

Each cluster has its unique infrared absorption spectrum and raman scattering spectrum determined by its composition and structures, so it can analyze and identify the clusters structures.

Infrared spectra is the generated of the vibrational energy level transition within the molecule, which is produced by the dipole moment change caused by the molecule during the vibration process, which reflects the vibration frequency of the molecule, and these frequencies are specific to each cluster. The harmonic frequency is greatly affected by the

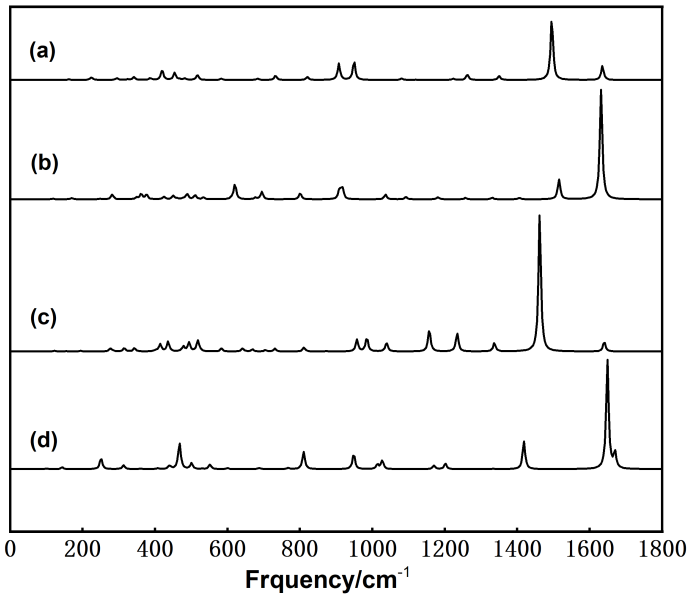

Figure 5: Infrared spectra. (a)$B_{10}N$; (b)$B_{11}N$; (c)$B_{12}N$; (d)$B_{13}N$.

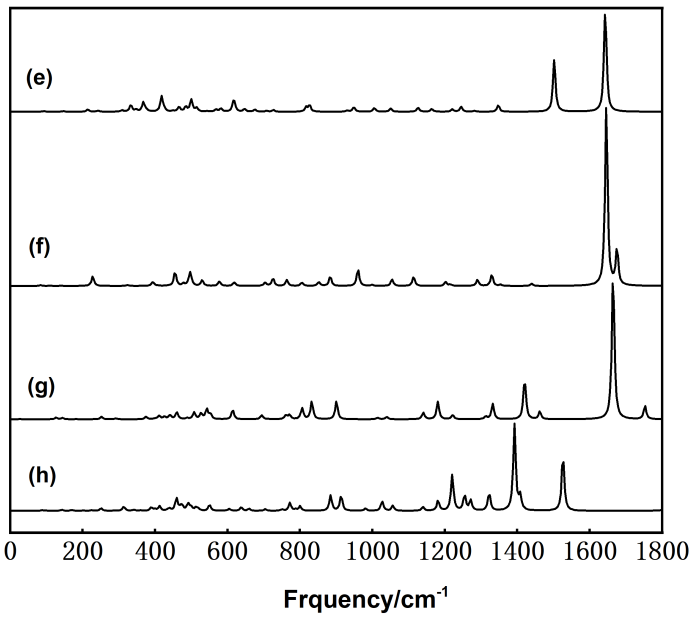

Figure 6: Infrared spectra. (e)$B_{14}N$; (f)$B_{15}N$; (g)$B_{16}N$; (h)$B_{17}N$.

cluster structure, because the stretching or bending vibration of atoms is the source of vibration patterns. Small differences in molecular structures can cause subtle changes in the normal pattern of vibration.

Figure 5, Figure 6 and Figure S4 (Support Information) show spectra plot of the strongest infrared active vibration modes of the calculated B_nN clusters ($n = 10-20$) at the PBE0 level with 6-311G(D) basit set. In the 27 vibration modes of $B_{10}N$, 23 of them are vibrational modes with infrared activity, and 4 of them are non-active, its strongest peak is located at a frequency of 1495 cm^{-1}. In the 30 vibration modes of $B_{11}N$, there are 29 vibration modes with infrared activity, 1 vibration mode without infrared activity, its strongest peak is located at 1631 cm^{-1}. In the 33 vibration modes of $B_{12}N$, there are 25 vibration modes with infrared activity, 8 vibration modes without infrared activity, its strongest peak is located at a frequency of 1462 cm^{-1}. In the 36 vibration modes of $B_{13}N$, there are 22 vibration modes with infrared activity, 14 vibration modes without infrared activity, its strongest peak is located at a frequency of 1649 cm^{-1}. In the 39 vibration modes of $B_{14}N$, there are 37 vibration modes with infrared activity, 2 vibration modes without infrared activity, its strongest peak is located at a frequency of 1643 cm^{-1}. In the 42 vibration modes of $B_{15}N$, there are 28 vibration modes with infrared activity, 14 vibration modes without infrared activity, its strongest peak is located at a frequency of 1646 cm^{-1}. In the 45 vibration modes of $B_{16}N$, there are 32 vibration modes with infrared activity, 13 vibration modes without infrared activity, its strongest peak is located at 1665 cm^{-1}. In the 48 vibration modes of $B_{17}N$, there are 37 vibration modes with infrared activity, 11 vibration modes without infrared activity, its strongest peak is located at a frequency of 1392 cm^{-1}. In the 51 vibration modes of $B_{18}N$, there are 34 vibration modes with infrared activity, 17 vibration modes without infrared activity, its strongest peak is located at a frequency of 1404 cm^{-1}. In the 54 vibration modes of $B_{19}N$, there are 36 vibration modes with infrared activity, 18 vibration modes without infrared activity, its strongest peak is located at a frequency of 1613 cm^{-1}. In the 57 vibration modes of $B_{20}N$, there are 32 vibration modes with infrared activity, 25 vibration modes without infrared activity, its strongest peak is located at a frequency of 1512 cm^{-1}.

Raman spectrum is generated by a change in the polarization rate of a molecule in a

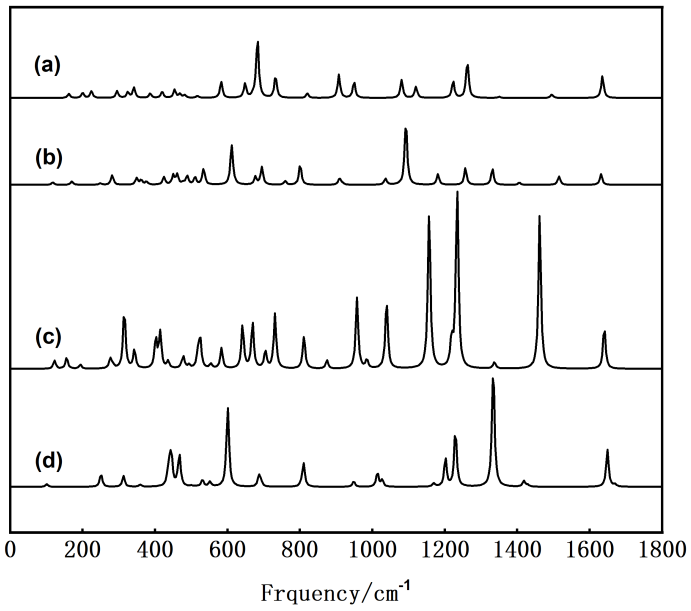

Figure 7: Raman spectra. (a)$B_{10}N$; (b)$B_{11}N$; (c)$B_{12}N$; (d)$B_{13}N$.

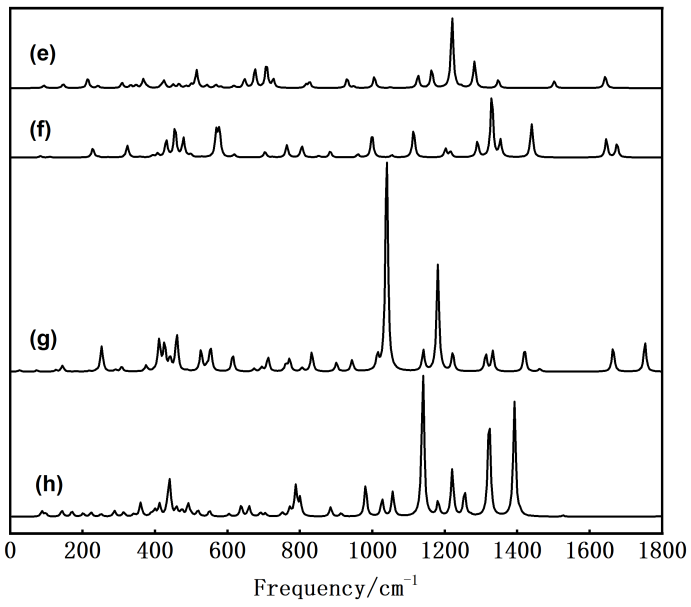

Figure 8: Raman spectra. (e)$B_{14}N$; (f)$B_{15}N$; (g)$B_{16}N$; (h)$B_{17}N$.

fixed direction during vibration. In addition, according to the calculation results in Figure 7 , Figure 8 and Figure S5 (Support Information). In the 27 vibration modes of $B_{10}N$, there are 26 vibration modes with raman activity, 1 vibration modes is no activity, its strongest peak is situated at 683 cm^{-1}. In the 30 vibration modes of $B_{11}N$, there are 28 vibration modes with raman activity, 2 vibration modes are no activity, its strongest peak is situated at 1092 cm^{-1}. In the 30 vibration modes of $B_{12}N$, there are 29 vibration modes with raman activity, 4 vibration modes are no activity. The first and second strongest peaks with raman activity are situated at the 26th and 24th peaks at frequencies 1234 cm^{-1} and 1157 cm^{-1}, respectively. The 24th peak is created by the combination of 27 and 28 vibration modes. In the 36 vibration modes of $B_{13}N$, there are 23 vibration modes with raman activity, 13 vibration modes are no activity, its strongest peak is situated at 1334 cm^{-1}. In the 39 vibration modes of $B_{14}N$, there are 36 vibration modes with raman activity, 3 vibration modes are no activity, its strongest peak is located at 1220 cm^{-1}. In the 42 vibration modes of $B_{15}N$, there are 35 vibration modes with raman activity, 7 vibration modes are no activity, its strongest peak is located at 1330 cm^{-1}. In the 45 vibration modes of $B_{16}N$, there are 35 vibration modes with raman activity, 11 vibration modes are no activity, its strongest peak is situated at 1039 cm^{-1}. In the 48 vibration modes of $B_{17}N$, there are 42 vibration modes with raman activity, 6 vibration modes are no activity, its strongest peak is located at 1139 cm^{-1}. In the 51 vibration modes of $B_{18}N$, there are 37 vibration modes with raman activity and 14 vibration modes are no activity, the eighth peak is generated by the combination of a pair of degenerate vibration modes, its strongest peak is situated at 1092 cm^{-1}.

In the 54 vibration modes of $B_{19}N$, there are 37 vibration modes with raman activity, 17 vibration modes are no activity, its strongest peak is situated at 1334 cm^{-1}. In the 57 vibration modes of $B_{20}N$, there are 37 vibration modes with raman activity and 20 vibration modes are no activity, of which the 49th is a pair of degenerate vibration modes, its strongest peak is situated at 1321 cm^{-1}. The number of peaks included in the spectrogram is consistent with the number of vibrationally active modes, because only vibrationally active modes can produce peaks and form the spectra.

3.4 Electronic Absorption Spectra

The electronic absorption spectrum is generated by transition valence electrons. Through the electron absorption spectrum and degree of absorption of molecules or ions of the substance, its composition and structure can be analyzed and determined.

Table 3: The excitation characteristics of clusters $B_nN(n = 10 - 20)$.

	wavelength of of the excited state with the strongest oscillator strength	wavelength of the first excited state (oscillator strength)	wavelength of first absorption peak (corresponding excited state)
$B_{10}N$	304 nm (0.0283, 27)	1460 nm (0.0004)	300 nm (28)
$B_{11}N$	237 nm (0.1983, 31)	679 nm (0.0028)	237 nm (21)
$B_{12}N$	291 nm (0.0284, 36)	1733 nm (0.0056)	306 nm (31)
$B_{13}N$	236 nm (0.5750, 30)	808 nm (0)	233 nm (31)
$B_{14}N$	328 nm (0.0284, 29)	979 nm (0.0016)	332 nm (28)
$B_{15}N$	284 nm (0.2258, 21)	869 nm (0.0001)	279 nm (23)
$B_{16}N$	438 nm (0.1163, 19)	1385 nm (0.0001)	438 nm (19)
$B_{17}N$	301 nm (0.1484, 23)	848 nm (0.0003)	301 nm (23)
$B_{18}N$	454 nm (0.0669, 22)	1185 nm (0)	449 nm (23)
$B_{19}N$	290 nm (0.2461, 29)	814 nm (0.0016)	283 nm (30)
$B_{20}N$	500 nm (0.0228, 21)	1230 nm (0.0005)	477 nm (24)

According to the above calculations, we investigated adopting the PBE0 method with 6-311G(D) basis set to calulate electronic absorption spectrum of clusters $B_nN(n = 10 - 20)$ (excited energy E, wavelength λ, and vibrator strength f for the first 36 excited states). Figure 9, Figure 10, Figure 11 and Figure 12 show the electronic absorption spectrum of the closed shell structures and the open shell structures, respectively. It is that some excited state parameters are given in Table 3, the position of the peaks and the energy of the transition with maximum intensity do not always correspond. the wavelength from the first excited state of these clusters are extended to the infrared band except cluster $B_{11}N$. $B_{13}N$ and $B_{18}N$ are the inhibited excited state, because its vibrator strength is zero. The wavelength

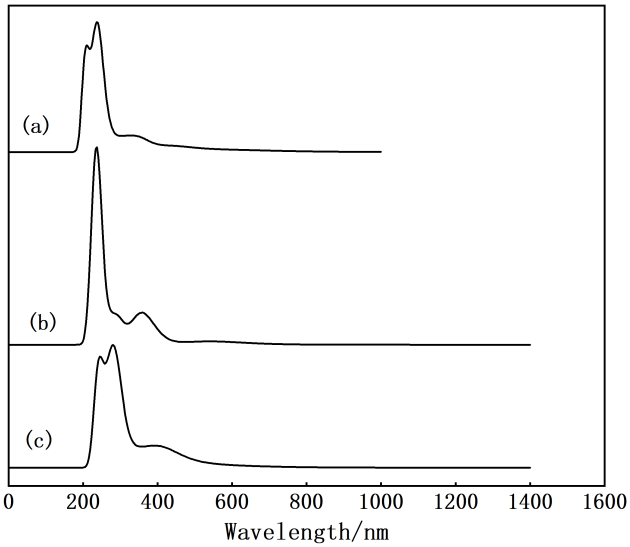

Figure 9: Calculated electronic absorption spectra of closed shell structures. (a)$B_{11}N$; (b)$B_{13}N$; (c)$B_{15}N$.

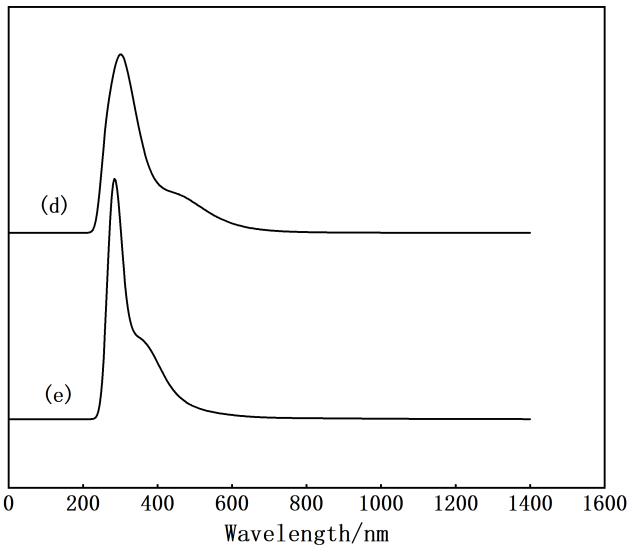

Figure 10: Calculated electronic absorption spectra of closed shell structures. (d)$B_{17}N$; (e)$B_{19}N$.

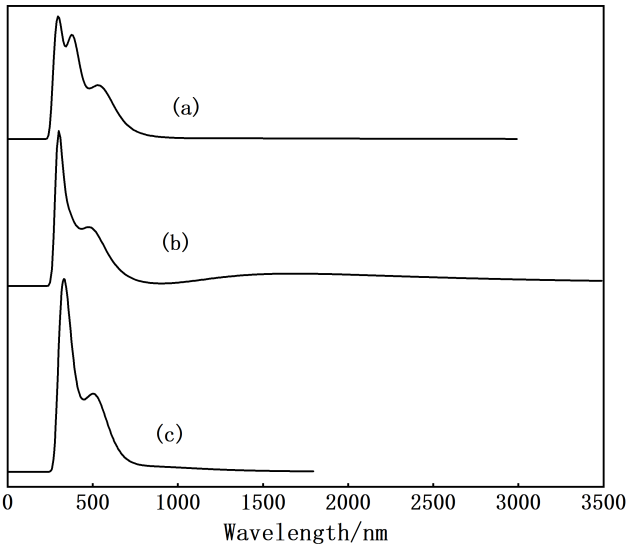

Figure 11: Calculated electronic absorption spectra of open shell structures. (a)$B_{10}N$; (b)$B_{12}N$; (c)$B_{14}N$.

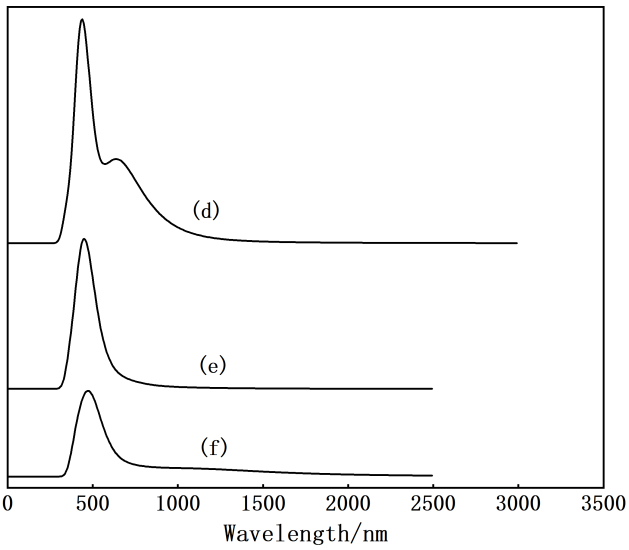

Figure 12: Calculated electronic absorption spectra of open shell structures. (d)$B_{16}N$; (e)$B_{18}N$; (f)$B_{20}N$.

corresponding to the first absorption peaks and the wavelength of the excitation state with the highest intensity of the oscillator of $B_nN(n = 10-20)$ are located in the ultraviolet-visible band. In addition, it can also be seen from Table 3 that in the clusters $B_nN(n = 10-20)$, the longest wavelength is $B_{12}N$ of the first excited state, while the shortest is $B_{11}N$.

It can be known from the graphs and tables drawn that the strongest absorption peak is not located in the wavelength position of the excited state with the highest vibrator strength except $B_{16}N$, $B_{17}N$. This can be seen for closed shell structures of $B_{11}N$, $B_{13}N$, and $B_{15}N$, they all have two absorption peaks, while for $B_{17}N$, $B_{19}N$, there is only one absorption peak. As can be seen from for open shell structures, $B_{10}N$ has three absorption peaks, $B_{12}N$, $B_{14}N$ and $B_{16}N$ they all have two absorption peaks, while for $B_{18}N$ and $B_{20}N$, there is only one absorption peak. The structures of these clusters can be identified from their UV-Vis spectral properties.

4. CONCLUSIONS

To sum up, we systematically study the lowest energy structures of the nitrogen-doped boron clusters BnN $(n = 10-20)$ by using ABCluster global search technique and particle swarm optimization (CALYPSO) software combined with Density functional method, and its size varies between 10 and 20. The ground-state properties, electron-delocalization characteristics, infrared, raman and electronic absorption spectra properities of the lowest energy structures are discussed. Its shows: (1) The lowest energy structures of B_nN $(n = 11, 13, 15-20)$ posses planar or quasi planar structures; $B_{10}N$ and $B_{12}N$ possess bowl-like structures; $B_{14}N$ possess a ship structure. The $B_{20}N$ of the planar structure is the most stable of all structures. (2) The energy gaps of $B_nN(n = 11, 13, 15, 17, 19)$ for the closed shell clusters reveal that the structure of $B_{19}N$ is most stable. (3) Chemical bonding analyses and NPA reveal that there are strong covalent bonds between boron atons and nitrogen atoms for $B_nN(n = 10-20)$ clusters and boron atoms sectional electrons transfer to doped nitrogen atoms. (4) Infrared and Raman spectra show that clusters $B_nN(n = 10-20)$ have a large number characteristic peaks, and the strongest IR peaks and Raman peaks are situated at different positions, which can be used to identify the clusters structures and make comparative analysis with

future experiments. (5) It can be obtained by analyzing the electronic absorption spectrum of clusters, the first absorption peak of the closed shell structures and the open shell structures are in the visible light band. The study provides theoretical guidance and basis for the development of novel boron based nanomaterials.

Supporting Information

Figure S1. The most metastable geometries of clusters $B_nN(n = 10 - 20)$.

Figure S2. LOL with the isosurface of 0.5 for $B_nN(n = 10 - 20)$.

Figure S3. ELF with the isosurface of 0.8 for $B_nN(n = 10 - 20)$.

Figure S4. IR Spectra of clusters $B_nN(n = 18 - 20)$.

Figure S5. Raman Spectra of clusters $B_nN(n = 18 - 20)$.

ACKNOWLEDGMENTS

This work was supported by the National Natural Science Foundation of China (Grant No:11804065), the Growth Foundation for Young Scientists of Education Department of Guizhou Province, China (Grant No: QJH KY[2022]310).

References

1. Ruan, W., Yu, X.-G., Xie, A.-D., Wu, D.-L., Luo, W.-L., Acta. Physica. Sinica., **2014**, 63 (24).

2. Tai, T. B., Tam, N. M., Nguyen, M. T., Chemical. Physics. Letters., **2012**, 530, 71-76.

3. Lu, Q. L., Luo, Q. Q., Li, Y. D., The European. Physical. Journal. D., **2018**, 72 (6).

4. Tuyet Mai, D. T., Van Duong, L., Pham-Ho, M. P., Nguyen, M. T., The Journal. of Physical. Chemistry. C., **2020**, 124 (12), 6770-6783.

5. Chen, W. J., Kulichenko, M., Choi, H. W., Cavanagh, J., Yuan, D. F., Boldyrev, A. I., Wang, L. S., J. Phys. Chem. A., **2021**, 125 (31), 6751-6760.

6. Tai, T. B., Nguyen, M. T., Chem. Commun (Camb)., **2015**, 51 (36), 7677-7680.

7. Tian, Y., Wei, D., Jin, Y., Barroso, J., Lu, C., Merino, G., Phys. Chem. Chem. Phys., **2019**, 21 (13), 6935-6941.

8. Li, P., Du, X., Wang, J. J., Lu, C., Chen, H., The Journal. of Physical. Chemistry. C., **2018**, 122 (34), 20000-20005.

9. Zhao, L., Qu, X., Wang, Y., Lv, J., Zhang, L., Hu, Z., Gu, G., Ma, Y., J. Phys. Condens. Matter., **2017**, 29 (26).

10. Li, S. X., Zhang, Z. P., Long, Z. W., Chen, D. L., ACS Omega., **2020**, 5 (32), 20525-20534.

11. Li, S.-X., Zhang, Z.-P., Long, Z.-W., Qin, S.-J., RSC Advances., **2017**, 7 (61), 38526-38537.

12. Tai, T. B., Lee, S. U., Nguyen, M. T., Phys. Chem. Chem. Phys., **2016**, 18 (17), 11620-11623.

13. Tai, T. B., Nguyen, M. T., Phys. Chem. Chem. Phys., **2015**, 17 (20), 13672-13679.

14. Yang, Y., Zhang, Z., Penev, E. S., Yakobson, B. I., Nanoscale., **2017**, 9 (5), 1805-1810.

15. Pham, H. T., Duong, L. V., Tam, N. M., Pham-Ho, M. P., Nguyen, M. T., Chemical. Physics. Letters., **2014**, 608, 295-302.

16. Popov, I. A., Jian, T., Lopez, G. V., Boldyrev, A. I., Wang, L. S., Nat Commun., **2015**, 6.

17. Liang, W. Y., Das, A., Dong, X., Cui, Z. H., Phys. Chem. Chem. Phys., **2018**, 20 (23), 16202-16208.

18. Jin, S., Chen, B., Kuang, X., Lu, C., Gutsev, G. L., J. Phys. Condens. Matter., **2019**, 31 (48).

19. Saha, P., Rahane, A. B., Kumar, V., Sukumar, N., The Journal. of Physical. Chemistry. C., **2017**, 121 (20), 10728-10742.

20. Lv, J., Wang, Y., Zhang, L., Lin, H., Zhao, J., Ma, Y., Nanoscale., **2015**, 7 (23), 10482-10489.

21. Li, W. L., Romanescu, C., Galeev, T. R., Piazza, Z. A., Boldyrev, A. I., Wang, L. S., J. Am. Chem. Soc., **2012**, 134 (1), 165-168.

22. Li, P., Mei, T., Lv, L.; Lu, C., Wang, W., Bao, G., Gutsev, G. L., J. Phys. Chem. A., **2017**, 121 (34), 6510-6516.

23. Tai, T. B., Kadlubanski, P., Roszak, S., Majumdar, D., Leszczynski, J., Nguyen, M. T., Chem. Phys. Chem., **2011**, 12 (16), 2948-2958.

24. Yang, Y. J., Li, S. X., Chen, D. L., Long, Z. W., ACS Omega., **2021**, 6 (45), 30442-30450.

25. Gu, J., Wang, C., Cheng, Y., Zhang, L., Yang, X., Computational and Theoretical Chemistry., **2014**, 1049, 67-74.

26. Gu, J.-B., Yang, X.-D., Wang, H.-Q., Li, H.-F., Chinese. Physics. B., **2012**, 21 (4).

27. Liu, Z.-F., Lei, X.-L., Liu, L.-R., Liu, H.-Y., Zhu, H.-J., Chinese. Physics. B., **2011**, 20 (2).

28. Piazza, Z. A., Hu, H. S., Li, W. L., Zhao, Y. F., Li, J., Wang, L. S., Nat Commun., **2014**, 5.

29. Saha, P., Rahane, A. B., Kumar, V., Sukumar, N., Physica. Scripta., **2016**, 91 (5).

30. Zhang, J., Dolg, M., Phys. Chem. Chem. Phys., **2016**, 18 (4), 3003-3010.

31. He, R., Zeng, X. C., Chem. Commun (Camb)., **2015**, 51 (15), 3185-3188.

32. Chen, Q., Wei, G. F., Tian, W. J., Bai, H., Liu, Z. P., Zhai, H. J., Li, S. D., Phys. Chem. Chem. Phys., **2014**, 16 (34), 18282-18287.

33. Chacko, S., Kanhere, D. G., Boustani, I., Physical. Review. B., **2003**, 68 (3).

34. Romanescu, C., Galeev, T. R., Li, W. L., Boldyrev, A. I., Wang, L. S., Accounts. of Chemical. Research., **2013**, 46 (2), 350-358.

35. Chen, T. T., Cheung, L. F., Wang, L. S., Annual. Review. of Physical. Chemistry., **2022**, 73, 233-253.

36. Tan Pham, H., Nguyen, M. T., J. Phys. Chem. A., **2019**, 123 (38), 8170-8178.

37. Li, P., Du, X., Wang, J. J., Lu, C., Chen, H., The Journal. of Physical. Chemistry. C., **2018**, 122 (34), 20000-20005.

38. Tai, T. B., Nguyen, M. T., Chem. Commun (Camb)., **2015**, 51 (36), 7677-7680.

39. Adamo, C., Barone, V., Journal. of Chemical. Physics., **1999**, 110 (13), 6158-6170.

40. Lv, J., Wang, Y., Zhang, L., Lin, H., Zhao, J., Ma, Y., Nanoscale., **2015**, 7 (23), 10482-10489.

41. Romanescu, C.; Galeev, T. R.; Li, W. L.; Boldyrev, A. I.; Wang, L. S. Aromatic metal-centered monocyclic boron rings: Co©B_8^- and Ru©B_9^-. Angew. Chem. Int. Ed. Engl., **2011**, 50 (40), 9334-9337.

42. Jian, T., Chen, X., Li, S. D., Boldyrev, A. I., Li, J., Wang, L. S., Chem. Soc. Rev., **2019**, 48 (13), 3550-3591.

43. Sergeeva, A. P., Popov, I. A., Piazza, Z. A., Li, W. L., Romanescu, C., Wang, L. S., Boldyrev, A. I., Acc. Chem. Res., **2014**, 47 (4), 1349-1358.

44. Lu, T., Chen, F., J. Comput. Chem., **2012**, 33 (5), 580-592.

45. Becke, A. D., Edgecombe, K. E., The Journal. of Chemical. Physics., **1990**, 92 (9), 5397-5403.

46. Mackoy, T., Kale, B., Papka, M. E., Wheeler, R. A., Computer. Physics. Communications., **2021**, 264.

47. A, Savin, B., Silvi, F. C., Canadian. Journal. of Chemistry., **1996**, 74.

48. Bai, H., Chen, Q., Zhai, H. J., Li, S. D., Angew. Chem. Int. Ed. Engl., **2015**, 54 (3), 941-945.

49. Chen, Q., Li, H. R., Tian, W. J., Lu, H. G., Zhai, H. J., Li, S. D., Phys. Chem. Chem. Phys., **2016**, 18 (21), 14186-14190.

50. Zhang, J., Dolg, M., Chem. Chem. Phys. **2015**, 17, 24173-24181.

51. Zhang, J., Dolg, M., Phys. Chem. Chem. Phys. **2016**, 18, 3003-3010.

52. Zhang, J., Glezakou, V.-A., Rousseau, R., Nguyen, M.-T., J. Chem. Theory Comput., **2020**,16, 3947-3958.

53. J. Lv, Y., Wang, L. Zhu and Y., Ma, J. Chem. Phys., **2012**, 137, 084104.

54. Frisch, M. J., Schlegel, H. B., Scuseria, G. E., Robb, M. A., Cheeseman, J. R., Montgomery, J. A., Vreven, T., Kudin, K. N., Burant, J. C., Millam, J., CT, **2009**.

55. Hao, Y. R., Bai, T. T., Jia, L. N., Xin, W., Hu, Y. F., Zheng, X. S., Hou, S. T., The Journal. of Physical. Chemistry. C., **2019**, 123 (47), 28561-28568.

56. Xia, X. X., Hermann, A., Kuang, X. Y., Jin, Y. Y., Lu, C., Xing, X. D., Journal. of Physical. Chemistry. C., **2016**, 120 (1), 677-684.

57. Le Chen, B., Sun, W. G., Kuang, X. Y., Lu, C., Xia, X. X., Shi, H. X., Maroulis, G., Inorg. Chem., **2018**, 57 (1), 343-350.

58. Wu, G., Wang, J., Zhang, X., Zhu, L., The Journal. of Physical. Chemistry. C., **2009**, 113 (17), 7052-7057.

59. He, R., Zeng, X. C., Chem. Commun (Camb)., **2015**, 51 (15), 3185-3188.